Ordering of monodisperse Ni nanoclusters by templating on high-temperature reconstructed α-Al$_2$O$_3$(0001)

K Venkataramani[1], S Helveg[2], B Hinnemann[2], M Reichling[3], F Besenbacher[1] and J V Lauritsen[1]

[1] Interdisciplinary Nanoscience Center (iNANO) and Department of Physics and Astronomy,
Aarhus University, Aarhus C, DK 8000, Denmark
[2] Haldor Topsøe A/S, 2800 Kongens Lyngby, Denmark
[3] Fachbereich Physik, Universität Osnabrück, 49076 Osnabrück, Germany

E-mail: jvang@inano.au.dk

Abstract
We demonstrate that the characteristic $\sqrt{31} \times \sqrt{31}$ $R9°$ reconstructed surface of α-alumina (Al$_2$O$_3$) acts as a nanotemplate for the growth of well-ordered monodisperse arrays of Ni nanoclusters. Due to the insulating nature of the substrate we use dynamic scanning force microscopy operated in the non-contact mode (NC-AFM) to characterize the nanotemplate, to examine the size and distribution of metallic clusters on the surface and to investigate their position with respect to the surface atomic structure. The present NC-AFM results for the interaction of Ni with α-Al$_2$O$_3$ are supported by density functional theory (DFT) calculations. The ability of α-Al$_2$O$_3$(0001) to act as a nanotemplate is attributed to a spatially modulated affinity towards the accommodation of Ni into the top layer by substituting the surface Al atoms at certain sites on the $\sqrt{31} \times \sqrt{31}$ $R9°$ reconstructed surface formed by high-temperature annealing. The insulating template, demonstrated for Al$_2$O$_3$, may be a generally attractive system for the study of nanostructures which need to be isolated from a conducting bulk.

(Some figures in this article are in colour only in the electronic version)

1. Introduction

Achieving periodic ordering of nanoscale structures within a particular medium has been the goal of many efforts since such systems are fundamentally interesting with respect to novel device applications such as high-density magnetic storage media [1] and spin-transport applications [2]. In recent years several examples of nanostructured surfaces that serve as templates for the growth of well-ordered arrays of monodisperse nanoclusters have been presented [3–6]. The research on such systems is mainly driven by the fundamental interest in controlling properties of matter as a function of structure and size, since unique size-dependent optical, magnetic, chemical (catalytic) or mechanical properties may arise when matter is confined to a size at the nanometre scale [7–9]. A range of bottom-up methods that explicitly make use of the intrinsic atomic-scale properties of certain substrates to achieve the synthesis of a nanoscale periodic array of nanoclusters with a high degree of spatial order have been developed. A network of surface–lattice dislocations [11] and a periodic pattern of dislocations [5, 12] formed as a result of lattice mismatch when one monolayer of a material is grown on top of another with a different lattice constant, and act as preferential nucleation centers for deposited metal atoms resulting in ordered nanostructure arrays on the substrate [13]. Specific nanostructures of the substrate are also used as a template for achieving ordered arrays of nanostructures such as growing ordered arrays of metal clusters on thin oxide films. Several studies have been dedicated to well-ordered substrates which were successfully obtained by growing ultra-thin oxide films on metallic substrates, e.g. [14, 15]. Surface reconstructions which are formed due to lattice mismatch of the thin film oxide overlayer with the metallic substrate have been shown to act as nucleation centres for the adsorbed metal

atoms, thereby creating monodispersed ordered nanoscale structures on the substrate [3, 6, 10, 16, 17]. Most previous studies have focused on template-assisted growth of metal nanoclusters on thin film oxides or nitrides [18] formed on a metal support. However, from a fundamental and application perspective it is of great relevance also to be able to investigate self-assembled nanocluster arrays which are genuinely electronically decoupled from a large conducting bulk, i.e. synthesized on the surface of bulk insulators [19]. The method of choice for the investigation of nanoparticles on a truly insulating surface is atomic force microscopy operated in the non-contact mode (NC-AFM) [20, 21], also known as dynamic scanning force microscopy (SFM). The technique has great potential for imaging and manipulating bulk insulating surfaces, specifically oxides with atomic resolution [22–24] and nanoclusters supported on such surfaces with nanoscale resolution [25–27]. Imaging nanoclusters with NC-AFM is, however, not trivial as the tip shape may strongly affect the apparent shape of the small clusters investigated [28, 29]. Using NC-AFM, we have recently successfully investigated the detailed growth and morphology of Cu nanoclusters on differently prepared α-Al$_2$O$_3$(0001) surfaces [25].

In this study, we characterize the growth of highly uniform ensembles of Ni nanoclusters on the reconstructed surface of a bulk insulating oxide, namely the $\sqrt{31} \times \sqrt{31}$ $R9°$ reconstructed surface of α-Al$_2$O$_3$(0001) by means of NC-AFM. By a detailed interplay between atomic-scale insight from NC-AFM experiments and first-principles density functional theory calculations (DFT), we investigate the ability of the surface to act as a template for the growth of ordered nanoscale arrays of Ni nanoclusters driven by a strongly modulated affinity for Ni to become embedded at particular atomic sites within the large unit cell of the reconstructed surface. In future, the intriguing template effect of the insulating Al$_2$O$_3$ surface may offer the possibility to study specific magnetic or catalytic properties of well-characterized ensembles of almost monodisperse Ni (or other inorganic, metallic, metal oxide or metal sulfide) nanoclusters.

2. Methods

2.1. Experimental details

Experiments were carried out in an ultra-high vacuum (UHV) system with a base pressure in the low 10^{-10} mbar range. The sample was a (0001)-oriented single crystal of α-Al$_2$O$_3$ with the dimensions 10 mm $\times$ 2 mm $\times$ 0.5 mm (MTI Corporation, Richmond, CA, USA) which was cleaned *ex situ* in 35% HNO$_3$ for 30 min, rinsed thoroughly in water and then annealed in air at 1200 °C for about 8 h. The crystal was then subjected to more than ten cycles of Ar$^+$ ion sputtering (1500 eV, 15 min) and annealing (1200 °C, 15 min) in ultra-high vacuum (UHV) to obtain a clean surface with atomically flat terraces. Annealing at this temperature was achieved by passing a current of about 6 A through a tungsten foil (0.01 mm thickness) clamped in between the α-Al$_2$O$_3$(0001) sample crystal and another Al$_2$O$_3$ crystal that was the insulating backside support for the sample holder.

The temperature was measured by observing the front of the crystal using an optical pyrometer (Metis MY81, Sensortherm GmbH, Sulzbach, Germany) that had been calibrated in the temperature range up to 800 °C against a thermocouple reading that was placed in direct contact with a test sample. After the initial cleaning, a single cleaning cycle prior to each experiment was sufficient to produce an impurity-free surface suitable for deposition experiments. This preparation procedure has previously been shown to lead to the formation of so-called high-temperature surface reconstruction defined by a $\sqrt{31} \times \sqrt{31}$ $R9°$ unit cell [30] as shown in figure 1(a). An atomistic model was recently established for the clean $\sqrt{31} \times \sqrt{31}$ $R9°$ surface using NC-AFM [30]. Ni was deposited on the clean reconstructed surface under UHV conditions at room temperature by electron-beam (e-beam)-assisted evaporation using a mini-e-beam evaporator (Oxford Applied Research, EGN4) of the Ni rod (99.99% purity), with a flux rate of $\sim$0.04 ML min^{-1} kept constant for all deposition experiments. To ensure deposition of mainly neutral metal Ni atoms, a grid inside the e-beam evaporator was positively biased by a few hundred volts against the Ni rod, thus repelling the small fraction of ionized Ni atoms. Prior to experiments, the Ni source was thoroughly outgassed for several hours so that the pressure in the UHV chamber never exceeded 6×10^{-10} mbar during evaporation. The total coverage of Ni on the surface was estimated from the NC-AFM images, and the obtained value was checked against deposition experiments on an Au(111) surface, serving as a reliable reference system (see [31]) for estimating the Ni coverage from STM images obtained in the same experimental set-up since tip-broadening is typically less severe in STM images on the two layer Ni islands that form on Au(111).

NC-AFM measurements were performed with a variable-temperature NC-AFM system (VT STM/AFM, Omicron GmbH, Taunusstein, Germany), but the signal processing was enhanced by the use of an easyPLL demodulator (NanoSurf, Liestal, Switzerland). As force sensors, we used commercial uncoated silicon cantilevers with a nominal tip radius of about 2 nm (Super Sharp Silicon NCH type, Nanosensors, Neuchâtel, Switzerland) with resonance frequencies in the range of 280–330 kHz and a spring constant of about 19 N m^{-1} that were excited to a stabilized oscillation with a peak-to-peak amplitude of about 20 nm. Deposited Ni clusters were imaged in the constant detuning mode in which a feedback loop controls the tip–surface distance in order to maintain a preset frequency detuning (df), a procedure basically reproducing the surface topography, in contrast to the constant height mode that is well suited for revealing atomic details on a flat terrace. The bias voltage applied between the tip and the sample support, U_{bias}[4], was monitored regularly and adjusted to minimize the electrostatic forces arising from the contact potential difference as described in [32]. After Ni deposition, we usually observed a slight rise in surface potential pointing to the build-up of a small amount of charge. To remove the unwanted charge, which is a potential obstacle for atomic resolution in NC-AFM, the sample was exposed to a short pulse (10 s, 0.2 mA

---

[4] The sign convention here is that U_{bias} is the potential applied to the surface relative to the tip.
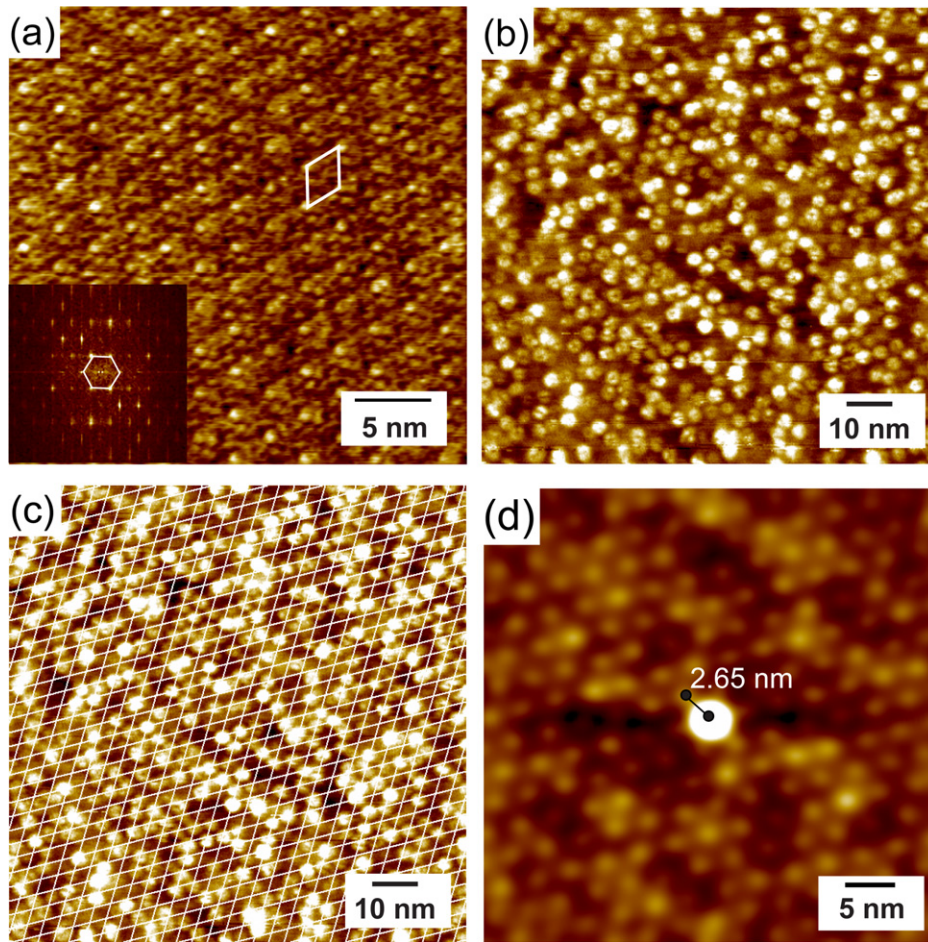
Figure 1. (a) A high-resolution NC-AFM image of the $\sqrt{31} \times \sqrt{31}$ $R9°$ reconstructed, clean α-Al$_2$O$_3$(0001) surface (imaging parameters: df $= -32$ Hz; size: 30×30 nm^2). The reconstruction unit cell is denoted by the white rhombus with a side length of 2.65 nm. The inset shows the corresponding 2D Fourier transform image exhibiting the surface periodicity. (b) NC-AFM image of Ni deposited at room temperature on the clean α-Al$_2$O$_3$(0001) surface. (c) Preferential nucleation of Ni clusters on the corners of the reconstruction unit cell represented by the white grid superimposed on the image from frame (b). (d) A zoom-in of the auto-correlation image of (b) demonstrating the 2.65 nm periodicity.

emission). The remaining potential difference (about 2–3 V) could always be fully compensated during scanning by adjusting the bias voltage (U_{bias}) accordingly.

2.2. Theory

DFT calculations have been carried out with the DFT code DACAPO [33], which uses a plane wave basis set and ultrasoft pseudopotentials [34]. A plane wave cutoff of 30 Ryd and a density cutoff of 45 Ryd have been used. The calculations have been carried out with the revised Perdew–Burke–Ernzerhoff (RPBE) functional [35] as the exchange–correlation functional. An electronic temperature of 0.1 eV was used with Fermi smearing, and all energies were extrapolated to zero electronic temperature. To represent α-Al$_2$O$_3$(0001), a (1 $\times$ 1) unit cell slab with a thickness of six stoichiometric layers is considered. As the Ni atoms were added to one side of the slab only, a correction for the slab dipoles is applied [36]. All atoms were relaxed until all force components were below 0.03 eV Å^{-1}. The only exception is the adsorption of a Ni atom on O$_{sub}$ position and substitution by

Ni atoms into the Al$_0$, Al$_1$ and Al$_3$ overlayer. This overlayer relaxes spontaneously to the O$_{sub}$ overlayer, and therefore its coordinates parallel to the surface were kept fixed, and it was only allowed to relax perpendicular to the surface. The calculations involving Ni have been carried out spin-polarized. The Ni adsorption energies are calculated as

$$\Delta E_{ads} = E(\text{Al}_2\text{O}_3 + \text{Ni}) - E(\text{Al}_2\text{O}_3) - E(\text{Ni, bulk}) \quad (1)$$

and the Ni substitution energies are calculated as

$$\Delta E_{sub} = E(\text{Al}_2\text{O}_3, \text{Ni}_{sub}) + E(\text{Al, bulk}) - E(\text{Al}_2\text{O}_3)$$
$$- E(\text{Ni, bulk}). \quad (2)$$

For further information on the details of the calculation, we refer to our previous work on α-Al$_2$O$_3$(0001) [30].

3. Results and discussion

The high-temperature phases of α-Al$_2$O$_3$(0001) are formed by annealing under vacuum conditions and have been studied by several techniques before [37, 38], including atom-resolved
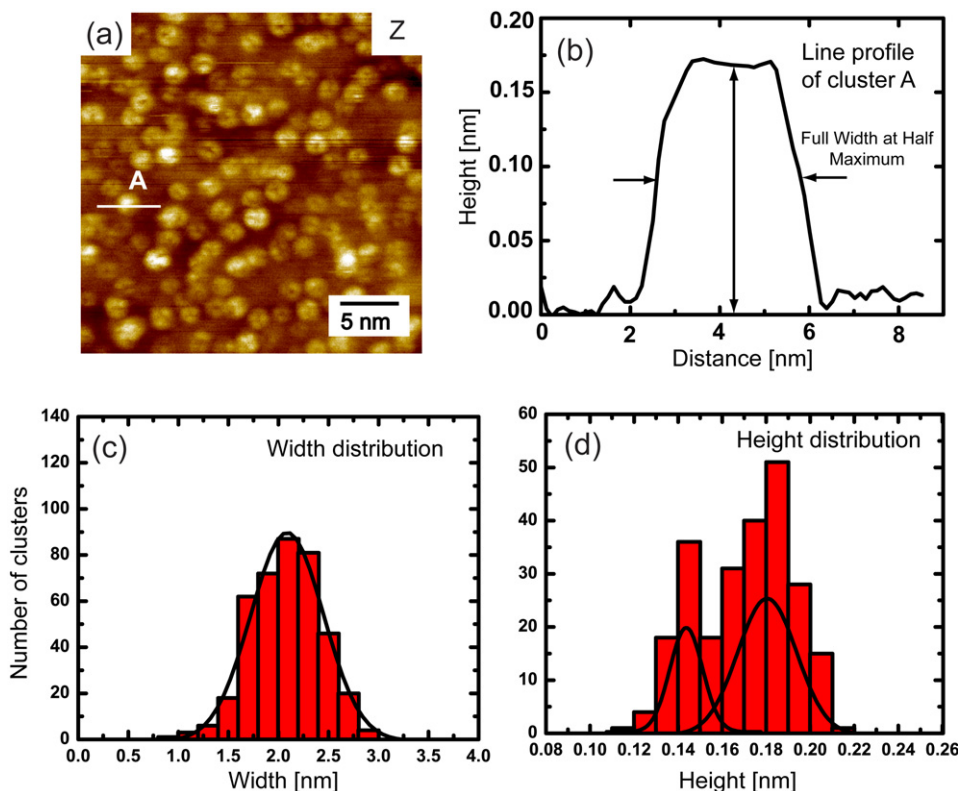
Figure 2. (a) NC-AFM image of Ni deposited on $\sqrt{31} \times \sqrt{31}$ $R9°$. (b) Line profile of Ni nanocluster marked A in frame (a), depicting the method employed for height and width measurement. (c) Width distribution of Ni nanoclusters derived from several NC-AFM images similar to the one shown in frame (a). (d) Bimodal height distribution of Ni nanoclusters derived from several NC-AFM images similar to the one shown in frame (a). The corresponding Gaussian fits to the distributions are represented by the black lines.

NC-AFM [30, 39]. At temperatures above 1200 °C, the surface has been shown to adopt the characteristic $\sqrt{31} \times \sqrt{31}$ $R9°$ reconstruction, which forms as a result of oxygen evaporation at such high temperatures, leading to an incommensurate Al-rich overlayer on top of the substrate [30, 38, 40]. The reconstruction is represented by a rhombic unit cell of dimensions 2.65 nm × 2.65 nm rotated by 9° with respect to the bulk unit cell. A high-resolution topographic NC-AFM image of the as-prepared, reconstructed surface prior to Ni deposition is shown in figure 1(a). Figure 1(b) shows a high-resolution topographic NC-AFM image of the surface after deposition of 0.18 ML of Ni. It is immediately apparent that the Ni deposition results in a uniform distribution of well-dispersed nanoclusters arranged in a hexagonally ordered pattern extending over the entire surface that apparently acts as a template for nanocluster growth.

To analyse the organization of Ni nanoclusters on the surface in detail, we show the image from frame (b) in figure 1(c) again but with a superimposed grid with precisely the orientation and dimension of the $\sqrt{31} \times \sqrt{31}$ $R9°$ reconstruction unit cell. We observe that almost all Ni nanoclusters are located at crossing positions of the grid, and, therefore, we conclude that the clusters adopt the characteristic 2.65 nm periodicity of the coincidence lattice structure of the reconstructed α-Al_2O_3(0001) surface. Figure 1(d) shows the auto-correlation function of frame (b) exhibiting a long range hexagonal order with well-defined peaks having the expected

2.65 nm periodicity. The auto-correlation image also reveals that the Ni clusters occupy the available lattice sites on the hexagonal grid defined by the surface reconstruction with nearly equal probability.

The particle width and height distributions were obtained from the line profiles of a large number of Ni nanoclusters in the NC-AFM images. As an example, the line profile of a Ni nanocluster (A) in a high-resolution NC-AFM image (see figure 2(a)) is shown in figure 2(b). The height of the Ni nanoclusters was measured as the distance from the top facet of the cluster to the substrate beneath. The width estimate of the nanoclusters was obtained by measuring the full width at half-maximum from the line profile of the Ni nanoclusters as shown in figure 2(b). It can be seen from figure 2(c) that the width distribution is quite sharp. The average value of the width of the Ni nanoclusters was found to be 2.1 ± 0.3 nm. However, it is important to note that, in NC-AFM, the tip broadening effect as a result of tip–surface convolution influences the imaging of supported nanoclusters. In the topography images, the clusters may appear slightly larger than in reality since the imaged shape of the clusters is not purely a geometric phenomenon, but a convolution of the tip and cluster shape. Figure 2(d) shows the corresponding height distribution of the Ni nanoclusters. The height distribution is interestingly quite broad. The height distribution is not affected by tip–sample convolution effects. It is, however, worth noting that the height distribution is, in fact, bimodal consisting of a main peak at 0.18 ± 0.05 nm and
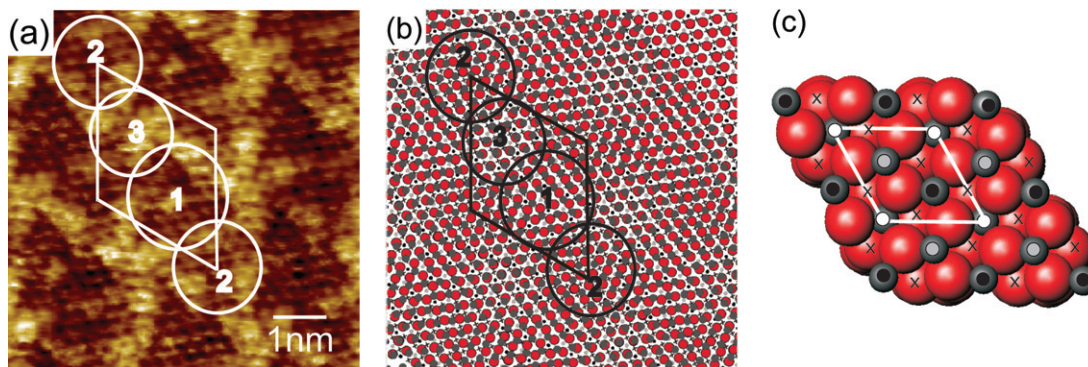
**Figure 3.** (Colour online) an atomically resolved NC-AFM image of the $\sqrt{31} \times \sqrt{31}$ $R9°$ reconstruction on α-Al$_2$O$_3$(0001) (imaging parameters: df = −24 Hz; size = 4 × 4 nm^2). The white rhombus denotes the reconstruction unit cell and the white circles enclose the three structurally different domains of the unit cell. (b) Schematic ball model of the surface atomic structure drawn at the same scale as the image of frame (a). Small light grey (grey in colour version) circles indicate Al atoms of the overlayer on top of the substrate. Large dark (red in colour version) circles indicate the surface O atoms of the substrate. (c) Top view of Al–Al–O–R-terminated (1 × 1) α-Al$_2$O$_3$ substrate with five different adsorption sites for possible Al occupation from the overlayer leading to the formation of three domains seen in frame (a). Large grey (red in colour version) spheres: O$_{top}$, large grey (red in colour version) spheres marked ×: O$_{sub}$, small grey spheres marked with black dot: Al$_0$, small grey spheres marked with grey dot: Al$_1$, small grey spheres marked with white dot: Al$_3$.

a minor peak at 0.15 ± 0.05 nm. The same variation in height is also directly visible in the NC-AFM image shown in figure 1(b) in which a significant number of Ni nanoclusters appear with a slightly lower contrast as compared to the other bright Ni nanoclusters. The variation in the height of the Ni nanoclusters by ~0.03 nm (a corrugation too low compared to the distance between two Ni(111) planes, which is ~0.21 nm) is tentatively attributed to adsorbates such as CO present on the top facet of some Ni nanoclusters due to adsorption from the background vacuum pressure. It has been previously observed that the adsorption of CO from the gas phase readily takes place on the Ni(111) surface at room temperature [41]. It is well known that in NC-AFM images the contrast formation for adsorbates strongly depends on the exact nature of the tip–surface distance and interactions, which in some cases even leads to a contrast inversion for the adsorbates [42]. Therefore, it is not possible to predict whether the presence of an adsorbate will increase or decrease the contrast in the corresponding NC-AFM image. Another peculiar effect is the apparent small depression present in most Ni nanoclusters (e.g. in figure 2(a)) which may be attributed to the contrast inversion phenomena related to the presence of adsorbates on top of the clusters [23, 43].

The average volume of the Ni nanoclusters can be estimated from the cluster dimensions obtained from the NC-AFM images and by assuming the same density as that of bulk fcc nickel and a layer density of atoms similar to an Ni(111) layer. Due to tip broadening which is always present when imaging three-dimensional objects with AFM, the actual width of the Ni nanoclusters is smaller than the value estimated from the NC-AFM images (figure 2(c)) which in general can be taken as the upper limit to the real value. A direct calculation of the average number of atoms per Ni nanoclusters from the height and width gives about 90 atoms per cluster, but considering tip broadening, which can be up to 30% of the width, a considerably lower value of 30–60 atoms per cluster is more realistic. The morphology of Ni nanoclusters therefore reflects that of flat one-layer high 2D islands with a close-

packed crystallographic plane oriented in parallel with the Al$_2$O$_3$ substrate.

To understand the atomistic mechanisms leading to the spontaneous formation of the Ni nanocluster arrays, it is necessary to first consider the atomic structure of the $\sqrt{31} \times \sqrt{31}$ $R9°$ reconstruction present on the substrate in some detail. The starting point of our analysis is the recently presented structural model of the atomic-scale structure of the $\sqrt{31} \times \sqrt{31}$ $R9°$ [30]. Figure 3(a) shows a highly magnified atomically resolved NC-AFM image of the $\sqrt{31} \times \sqrt{31}$ $R9°$ reconstruction with the unit cell represented by the white rhombus. The emergence of the rather large $\sqrt{31} \times \sqrt{31}$ unit cell on the α-Al$_2$O$_3$(0001) surface is explained by evaporation of oxygen from the topmost layer of Al$_2$O$_3$ when the crystal is exposed to a temperature around 1200 °C [37, 38]. The resulting excess of Al leads to the formation of a compact, close-packed Al layer with a lattice spacing of 0.301 nm on top of the bulk-terminated α-Al$_2$O$_3$ surface (lattice constant = 0.275 nm) wetting the surface in a non-epitaxial manner. The detailed structure of the $\sqrt{31} \times \sqrt{31}$ $R9°$ reconstruction is explained in terms of the misfit pattern (a type of moiré structure) arising from the lattice mismatch of the hexagonally arranged Al overlayer relative to the Al$_2$O$_3$ substrate. A rotation by 32° of the overlayer with respect to the substrate beneath leads to the formation of the moiré structure comprising a distinct pattern of three domains, each with a periodicity of 2.65 nm. The atomically resolved NC-AFM image of the reconstructed clean surface comprising the three different domains (enclosed by numbered circles) is shown in figure 3(a). Figure 3(b) illustrates, in a schematic ball model, the structure of the overlayer atoms (small grey balls) on top of the stoichiometric α-Al$_2$O$_3$(0001) substrate with respect to the substrate, within the unit cell of the $\sqrt{31} \times \sqrt{31}$ $R9°$ reconstruction. This sketch illustrates how the expansion and rotation of the Al overlayer on top of the substrate leads to the placement of overlayer atoms in periodically modulated stacking domains. The atomic structure of the underlying
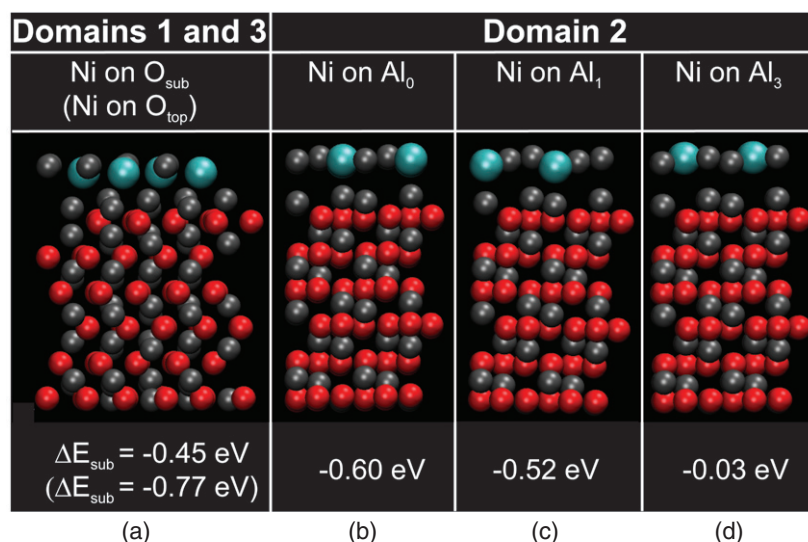
Figure 4. Side view of the DFT calculated surface structure models for substitution of surface Al atoms by Ni atoms in the three stacking domains. The respective energy gain for Ni substitution in each domain is indicated below the models. Ni substituted on (a) domains 1 and 3: on top of O_{top} and O_{sub} sites, (b)–(d) domain 2: on Al sites Al_0, Al_1 and Al_3, respectively. Large white spheres (light blue in colour version): Ni atoms, small dark grey spheres: Al atoms, small light grey spheres (red in colour version): O atoms.

substrate is depicted in figure 3(c). The substrate reflects the stoichiometric termination of the α-Al_2O_3(0001) surface with an additional Al layer, i.e. Al–Al-terminated surface of α-Al_2O_3 [30], and the ball model shows that the overlayer Al atoms can accommodate three distinctly different types of high-symmetry sites on this substrate. When placing an incommensurate Al overlayer on top of this substrate, the atoms occupy the three different sites in a periodically modulated manner, which gives rise to the imaging of the three different domains inside a single unit cell in the NC-AFM image. The exact stacking inside the three domains observed in the NC-AFM image could be resolved by their symmetry and variation in corrugation in the detailed comparison between atom-resolved images and structure simulations based on DFT [30]. Following the same notation, the first domain (1) reflects stacking predominantly on the hollow Al position of the substrate with the second O-layer lying directly below it (O_{sub}). The second domain (2) reflects Al atoms stacked on top of Al_0, Al_1 and Al_3 sites. Since the Al_0 and Al_1 sites are already occupied by Al atoms of the substrate, and the hollow Al_3 site is Al-deficient on the substrate, the overlayer Al atoms give rise to the appearance of the hexagonal feature (for example, see figure 3(c)) clearly observed in the atomically resolved NC-AFM images (see figure 3(a)). The third domain (3) is formed by Al atoms of the overlayer placed on the top position of the topmost O layer (O_{top}).

The repeat distance of the ordered Ni nanoclusters corresponds to the exact 2.65 nm periodicity of any one of the three domains, which implies that only one of the three domains contains the sites that can act as preferential nucleation sites for Ni during deposition. In order to investigate this effect in detail, DFT calculations of the energies involved in adsorption and substitution of surface Al atoms with Ni atoms in the three domains have been performed. Ni adsorption in the full $\sqrt{31} \times \sqrt{31}$ $R9°$ structure [30] was too large to

handle computationally, so in order to perform a simpler but still rather precise calculation and predict the trend for Ni interaction between the domains we have instead considered a regular (1×1) Al_2O_3 unit cell with an Al overlayer placed on top of each of the three sites corresponding closely to the geometry of each of the three domains. This theoretical method then estimates the Ni adsorption strength only near the centre of the three domains and not at the boundaries where the stacking is less well defined for the substrate. For all the three domains, adsorption of single Ni atoms into the Al overlayer was found to be endothermic by energies in the range from $E_{ads} = 0.2$ to 0.5 eV. On the other hand, the DFT calculations reveal that the substitution of surface Al atoms with Ni atoms in the Al overlayer on the different high-symmetry sites (i.e. O_{sub}, O_{top}, Al_0, Al_1 and Al_3) is strongly favoured compared to adsorption. Figure 4 shows the structure of the surface after the Al overlayer atoms are substituted by Ni atoms on different domains and their corresponding energies. As seen in figure 4(a) for Ni substituted in the first domain (1) (i.e. near Al hollow positions, O_{sub}) and the third domain (3) (i.e. on topmost O layer, O_{top}), the relaxed end configuration is exactly the same and Ni substitution is found to be exothermic by $E_{sub} = -0.45$ eV and -0.77 eV, respectively (see figure 4(a)). For Ni substitution in the second domain (2) as shown in figures 4(b)–(d), the energies are site-dependent since substitution into the Al overlayer on the Al_0 and Al_1 sites is calculated to be exothermic by -0.60 eV and -0.52 eV, respectively, and almost thermoneutral on Al_3. Since accommodation of Ni into the Al overlayer by substituting the Al atoms is favoured on all three domains and the energies are also similar in magnitude, the strong template effect of the reconstructed alumina surface cannot be directly rationalized from simple energy considerations. The template effect is, therefore, most likely related to strong kinetic effects involved in the accommodation of Ni into the surface which

may hinder/limit substitution of surface Al atoms with Ni in the other two domains, or due to preferential nucleation on a group of atomic sites not accounted for in the simple model. For instance, the current model does not describe the strain involved in forming the Al overlayer in the full unit cell $\sqrt{31} \times \sqrt{31}$ $R9°$. Also the additional strain energies could change the energetic picture in favour of one particular domain or, in particular, at the domain boundaries [6, 16]. The overall template effect can be explained by a mechanism where an incoming Ni atom replaces the surface Al atoms at a particular site. The Ni atoms that substituted the surface Al atoms then act as favourable sites for further Ni nucleation where Ni–Ni bonds dominate over Ni–Al bonds, and, therefore fosters the formation of stable Ni nanoclusters on the surface. This mechanism would be similar to that proposed previously for Ni on Au(111) where preferential Ni island formation takes place first through place exchange of Ni atoms with the Au substrate atoms and then the substituted Ni atoms act as preferential nucleation sites for further Ni adatoms [11, 44]. A similar effect has been observed earlier when the $\sqrt{31} \times \sqrt{31}$ $R9°$ reconstructed surface was exposed to water in UHV where the surface exhibited a preferential affinity for clustering of $Al(OH)_3$ at the corners of the rhombic unit cell [25, 39].

In order to investigate the thermal stability of the system, the Ni-deposited surface was subjected to annealing at temperatures ranging from room temperature to 600 °C for about 3 min at each temperature. From the subsequent NC-AFM images recorded (not shown), it was observed that the ordered arrays of Ni nanoclusters are stable until 350 °C. At higher annealing temperatures (350–500 °C), larger and fewer nanoclusters were observed, which suggest particle sintering either by Ostwald ripening, where large clusters grow at the expense of smaller ones, or by particle diffusion and coalescence [45]. At even higher annealing temperatures (>500 °C) no Ni nanoclusters were present on the surface. This dramatic decrease in the number density of Ni nanoclusters suggests a number of competing processes such as diffusion of Ni into the substrate [46] or desorption of Ni atoms from the surface.

To test the ability of the reconstructed α-Al_2O_3(0001) surface to act as a nanotemplate for the growth of other metals, the experiment was also extended to other transition metals. Deposition experiments were performed for Co and Mo on the same freshly prepared $\sqrt{31} \times \sqrt{31}$ $R9°$ α-Al_2O_3(0001) surface. However, in these preliminary sets of experiments we did not observe any ordered arrangement for Co and Mo. The modulated affinity for nucleation of metal clusters seems to be observed exclusively for Ni, which may be attributed to a very strong tendency of Ni and Al to form an alloy. In future, we will explore whether seeding with Ni atoms before deposition of other metals could be used to direct the template growth of a wider range of systems, as previously demonstrated for Fe deposition of thin alumina films on Ni_3Al(111) [47].

4. Summary

We have demonstrated the ability of the high-temperature reconstructed phase of α-Al_2O_3(0001) to grow nanostructured arrays of well-dispersed Ni nanoclusters with a long-range hexagonal order. It was found that one of the three domains present within the large rhombic unit cell of the superstructure acts as a preferential site where nucleation of Ni atoms is anticipated to begin. A two-stage nucleation and growth process is suggested. During the process the Ni atoms substitute the Al atoms in the overlayer at one of the preferred sites and then act as preferential nucleation sites for further Ni adatoms, forming stable 2D Ni nanoclusters.

Acknowledgments

References

[1] Sun S H, Murray C B, Weller D, Folks L and Moser A 2000 *Science* **287** 1989–92
[2] Black C T, Murray C B, Sandstrom R L and Sun S H 2000 *Science* **290** 1131–4
[3] Bäumer M and Freund H J 1999 *Prog. Surf. Sci.* **61** 127–98
[4] Degen S, Becker C and Wandelt K 2004 *Faraday Discuss.* **125** 343–56
[5] Brune H, Giovannini M, Bromann K and Kern K 1998 *Nature* **394** 451–3
[6] Berdunov N, Mariotto G, Balakrishnan K, Murphy S and Shvets I V 2006 *Surf. Sci.* **600** L287–90
[7] Valden M, Lai X and Goodman D W 1998 *Science* **281** 1647–50
[8] Link S and El-Sayed M A 2000 *Int. Rev. Phys. Chem.* **19** 409–53
[9] Haes A J, Haynes C L, McFarland A D, Schatz G C, Van Duyne R R and Zou S L 2005 *MRS Bull.* **30** 368–75
[10] Degen S, Becker C and Wandelt K 2003 *Faraday Discuss.* **125** 343–56
[11] Chambliss D D, Wilson R J and Chiang S 1991 *Phys. Rev. Lett.* **66** 1721–4
[12] Shiryaev S Y, Jensen F, Hansen J L, Petersen J W and Larsen A N 1997 *Phys. Rev. Lett.* **78** 503–6
[13] Morgenstern K, Kibsgaard J, Lauritsen J V, Lægsgaard E and Besenbacher F 2007 *Surf. Sci.* **601** 1967–72
[14] Kresse G, Schmid M, Napetschnig E, Shishkin M, Kohler L and Varga P 2005 *Science* **308** 1440–2
[15] Hamm G, Barth C, Becker C, Wandelt K and Henry C R 2006 *Phys. Rev. Lett.* **97** 126106
[16] Becker C, Rosenhahn A, Wiltner A, von Bergmann K, Schneider J, Pervan P, Milun M, Kralj M and Wandelt K 2002 *New J. Phys.* **4** 75
[17] Marsault M, Hamm G, Worz A, Sitja G, Barth C and Henry C R 2008 *Faraday Discuss.* **138** 407–20
[18] Corso M, Auwarter W, Muntwiler M, Tamai A, Greber T and Osterwalder J 2004 *Science* **303** 217–20
[19] Repp J, Meyer G, Paavilainen S, Olsson F E and Persson M 2006 *Science* **312** 1196–9

[20] Giessibl F J 1997 *Phys. Rev.* B **56** 16010–5
[21] Morita S W R and Meyer E 2002 *Non-Contact Atomic Force Microscopy* (New York: Springer)
[22] Foster A S, Barth C, Shluger A L, Nieminen R M and Reichling M 2002 *Phys. Rev.* B **66** 235417
[23] Hirth S, Ostendorf F and Reichling M 2006 *Nanotechnology* **17** S148–54
[24] Lauritsen J V and Reichling M 2010 *J. Phys.: Condens. Matter* at press
[25] Jensen M C R, Venkataramani K, Helveg S, Clausen B S, Reichling M, Besenbacher F and Lauritsen J V 2008 *J. Phys. Chem.* C **112** 16953–60
[26] Pang C L, Raza H, Haycock S A and Thornton G 2000 *Surf. Sci.* **460** L510–4
[27] Haas G, Menck A, Brune H, Barth J V, Venables J A and Kern K 2000 *Phys. Rev.* B **61** 11105–8
[28] Barth C and Henry C R 2004 *Nanotechnology* **15** 1264–72
[29] Pakarinen O H, Barth C, Foster A S and Henry C R 2008 *J. Appl. Phys.* **103** 076103
[30] Lauritsen J V, Jensen M C R, Venkataramani K, Hinnemann B, Helveg S, Clausen B S and Besenbacher F 2009 *Phys. Rev. Lett.* **103** 4
[31] Chambliss D D, Wilson R J and Chiang S 1991 *J. Vac. Sci. Technol.* B **9** 933–7
[32] Gritschneder S, Namai Y, Iwasawa Y and Reichling M 2005 *Nanotechnology* **16** S41–8
[33] The open source DFT code DACAPO is available at http://www.camd.dtu.dk/Software.aspx
[34] Vanderbilt D 1990 *Phys. Rev.* B **41** 7892–5
[35] Hammer B, Hansen L B and Nørskov J K 1999 *Phys. Rev.* B **59** 7413–21
[36] Bengtsson L 1999 *Phys. Rev.* B **59** 12301–4
[37] Renaud G, Villette B, Vilfan I and Bourret A 1994 *Phys. Rev. Lett.* **73** 1825–8
[38] French T M and Somorjai G A 1970 *J. Phys. Chem.* **74** 2489
[39] Barth C and Reichling M 2001 *Nature* **414** 54–7
[40] Chang C C 1968 *J. Appl. Phys.* **39** 5570
[41] Christma K, Ertl G and Schober O 1974 *Ber. Bunsen-Ges. Phys. Chem. Chem. Phys.* **78** 1262
[42] Rahe P, Bechstein R, Schütte J, Ostendorf F and Kühnle A 2008 *Phys. Rev.* B **77** 195410
[43] Meyer J A, Baikie I D, Kopatzki E and Behm R J 1996 *Surf. Sci.* **365** L647–51
[44] Gunter P L J, Niemantsverdriet J W, Ribeiro F H and Somorjai G A 1997 *Catal. Rev. Sci. Eng.* **39** 77–168
[45] Campbell C T, Parker S C and Starr D E 2002 *Science* **298** 811–4
[46] Winkler A, Borchert H and Al-Shamery K 2006 *Surf. Sci.* **600** 3036–44
[47] Schmid M, Kresse G, Buchsbaum A, Napetschnig E, Gritschneder S, Reichling M and Varga P 2007 *Phys. Rev. Lett.* **99** 196104